JOURNAL OF PETROLEUM AND MINING
مجلة النفط والتعدين

Numerical investigation of erosion in various oil-pipeline layouts using a discrete-phase model

Hudhaifa Hamzah [1,*], Nihad Saoud Aljuboori [1], Ibrahim Adil Ibrahim Al-Hafidh[1]

[1] *Department of Mining Engineering, College of Petroleum and Mining Engineering, University of Mosul, Iraq*

Article information

Article history:
Received Mar 11, 2026
Revised Jun 21, 2026
Accepted Jun 26, 2026
Available online Jul 01, 2026

Keywords:
CFD
Erosion
Pipeline configurations
Discrete phase model

Correspondence:
Hudhaifa Hamzah
hudhaifahamzah@gmail.com

ABSTRACT

The flow dynamics in pipes is a very complex system because it is significantly influenced by the flow conditions. The transportation of crude oil in pipelines within unconfined petroleum reservoirs is associated with the presence of solid particles. These particles are often transported as dispersed phases during crude oil production and are therefore detrimental to the integrity of the pipe surface. This could lead to the occurrence of crevice corrosion due to pipe erosion. Related to the above discussion, this project aims to analyze crude oil dynamics during flow through the pipeline and identify erosion hotspots for different pipe bends. Therefore, the present work numerically illustrated the effect of turbulent crude oil flow in different pipe configurations on the erosion rate. A computational fluid dynamics (CFD) model combined with a discrete phase model (DPM) was employed in this study using ANSYS (2020R1). In the current study, four different angles were considered to represent oil pipe configurations. These angles are 45 °, 90 º, 135 °, and 180 º. The four pipe designs were named Case_1_(45º), Case_2_(90º), Case_3_(135º) and Case_4_(180º). Further, the effect of inlet velocity was studied from 20 m/s to 35 m/s. Results stated that among the examined cases, the Case_1_(45º) was the most erosion-prone case, while the Case_2_(90º) provided the best erosion resistance. At 35 m/s, the erosion rate of the Case_1_(45º) was about 24% higher than that of the Case_2_(90º), highlighting the strong influence of bend angle on pipeline wear.

DOI: ***********,

دراسة عددية للتآكل في تصميمات مختلفة لخطوط أنابيب النفط باستخدام نموذج الطور المنفصل

حذيفة حمزة [1*] نهاد سعود الجبوري [1] ابراهيم عادل ابراهيم الحافظ [1]

[1] قسم هندسة التعدين، كلية هندسة النفط والتعدين، جامعة الموصل، العراق*

معلومات الارشفة

تاريخ الارشفة:

تاريخ الاستلام: 11 آذار 2026

تاريخ المراجعة: 21 حزيران 2026

تاريخ القبول: 26 حزيران 2026

تاريخ النشر الالكتروني: 01 تموز 2026

الكلمات المفتاحية:

ديناميكيات الموائع الحسابية

التآكل

تكوينات خطوط الأنابيب

نموذج الطور المنفصل

المراسلة:

حذيفة حمزة

hudhaifahamzah@gmail.com

الملخص

تُعدّ ديناميكيات التدفق في الأنابيب نظامًا بالغ التعقيد نظرًا لتأثرها الكبير بظروف التدفق. يرتبط نقل النفط الخام في خطوط الأنابيب داخل مكامن النفط غير المحصورة بوجود جزيئات صلبة. غالبًا ما تُنقل هذه الجزيئات كأطوار مُشتتة أثناء إنتاج النفط الخام، مما يُلحق الضرر بسلامة سطح الأنبوب. قد يؤدي ذلك إلى حدوث تآكل شقوقي نتيجة لتآكل الأنبوب. في هذا السياق، يهدف هذا المشروع إلى تحليل ديناميكيات النفط الخام أثناء تدفقه عبر خط الأنابيب وتحديد نقاط التآكل الرئيسية في مختلف انحناءات الأنابيب. لذلك، يُوضح هذا العمل عدديًا تأثير تدفق النفط الخام المضطرب في تكوينات أنابيب مختلفة على معدل التآكل. استُخدم في هذه الدراسة نموذج ديناميكيات الموائع الحسابية (CFD) مُدمج مع نموذج الطور المنفصل (DPM) باستخدام برنامج ANSYS (2020R1). في هذه الدراسة، تمّ اعتماد أربع زوايا مختلفة لتمثيل تكوينات أنابيب النفط. هذه الزوايا هي 45°، 90°، 135°، و180°. سُميت تصاميم الأنابيب الأربعة: الحالة 1_(45°)، الحالة 2_(90°)، الحالة 3_(135°)، والحالة 4_(180°). علاوة على ذلك، دُرست تأثيرات سرعة التدفق الداخل من 20 م/ث إلى 35 م/ث. أشارت النتائج إلى أن الحالة 1_(45°) كانت الأكثر عرضة للتآكل من بين الحالات المدروسة، بينما أظهرت الحالة 2_(90°) أفضل مقاومة للتآكل. عند سرعة 35 م/ث، كان معدل التآكل في الحالة 1_(45°) أعلى بنحو 24% من معدله في الحالة 2_(90°)، مما يُبرز التأثير الكبير لزاوية الانحناء على تآكل خط الأنابيب.

DOI: ***********

Introduction

The transportation of crude oil through pipelines is a critical component of the global energy infrastructure, providing a safe, efficient, and cost-effective means of transporting vast quantities of hydrocarbons over long distances. However, the flow of crude oil through pipelines is often accompanied by erosive wear, which can lead to the degradation of pipeline components and pose significant operational and safety risks (Ejeh et al., 2020). Erosion in oil pipelines is primarily caused by the interaction between the flowing fluid and the pipeline walls, resulting in the removal of material from the pipe surface due to the abrasive action of solid particles entrained in the fluid. The severity of erosion depends on various factors, including the flow velocity, fluid properties, pipeline geometry, and particle characteristics (Wee & Yap, 2019).

In recent years, computational fluid dynamics (CFD) simulations have emerged as powerful tools for studying erosive wear in oil pipelines and evaluating the effectiveness of erosion control measures. Among the various numerical modelling techniques used in CFD

simulations, the discrete phase model (DPM) stands out for its ability to accurately capture the motion and interaction of discrete particles within the flowing fluid (Hamzah & Sahin, 2023). The objective of this study is to perform a comprehensive numerical analysis of erosion in different oil pipeline configurations using the discrete phase model. By simulating the flow of crude oil and solid particles through various pipeline geometries, including straight sections, bends, elbows, and tees, we aim to investigate the impact of flow conditions and geometric factors on erosive wear rates.

The study of erosion in pipes is vital across industries, especially in oil and gas, due to its implications on safety, operational efficiency, and environmental integrity. Erosion-induced thinning of pipe walls poses significant safety risks, increasing the likelihood of leaks and ruptures with potential environmental damage and human harm. Operational inefficiencies arise from flow disruptions, leading to decreased throughput and increased costs. Moreover, erosion necessitates costly maintenance activities and regulatory compliance efforts, impacting asset integrity and operational budgets. Understanding erosion mechanisms is crucial for optimising pipeline design, materials, and operational parameters, enabling proactive risk mitigation and ensuring the long-term reliability and sustainability of pipeline infrastructure (Shirazi et al., 2015).

Previous studies have extensively investigated erosion phenomena in oil pipelines, recognizing its critical implications for safety, operational efficiency, and environmental protection. These studies have utilized various numerical modeling techniques, including computational fluid dynamics (CFD), to analyze erosive wear in pipeline systems (Hamzah et al., 2025). Empirical erosion models, turbulence models, and discrete phase models have been employed to simulate fluid flow, particle transport, and erosion rates in different pipeline configurations. Research efforts have focused on characterizing erosion patterns, evaluating erosion mitigation strategies, and optimizing pipeline designs to minimize erosive wear and enhance asset integrity. While these studies have provided valuable insights into erosion mechanisms and factors influencing erosion rates, there remains a need for further investigation into the specific effects of pipeline geometry, flow conditions, and particle properties on erosion in oil pipelines.

When oil field development begins, it is almost a guarantee that sand will also be produced. This is a result of the initial phase of fluid withdrawal in which the formation is disturbed, and sand grains are mechanically dislodged. The produced fluid transports these grains to the surface processing facilities where they experience a continued erosion. This erosion, the result of repeated impacts with the abrasive material and the metal of the processing equipment is known as sand erosion and is a cause of significant erosion of the processing equipment, increased costs due to more frequent maintenance and replacement, and in some cases, equipment failure. Notably, sand erosion is a complex problem with many contributing, and some conflicting, parameters. Over the years \cite{lehner2020sands}, many sand erosion models focused on various parameters have been published. In a review of 28 published papers on sand erosion found 33 different parameters of influence. This resulted in an average of 5 different parameters per model (Ludema, 1995).

Erosion is the result of a peculiar combination that includes the solid particles, fluid, walls, and flow. Of these, the size of the particles, especially sand size, has received the most research attention. Studies show that a unit increase in sand size yields an erosion rate, where the size of n typically ranges from 0.3 to 2.0 (Mcl Clark, 1991). Most of these studies have been performed on sand of sizes varying from 100 to 700 μm. Traditionally, sand particles

smaller than 100 μm have a lower kinetic energy and have been traditionally ignored. Under very high flow conditions, they also contribute to erosion. For instance, (Kesana, 2013) noted significant erosion in a standard elbow from 20 μm sand particles. Furthermore, even after the numerous in situ sand control measures, fine particles, typically less than 75 μm, travel to the surface and contribute to erosion of the pipes and endanger the integrity of the system (Subramani et al., 2014). In the real world, particle sizes are variable and consist of a wide range of diameters. Even though this variability exists, most erosion models oversimplify the phenomenon by assuming the particle population consists of a single size. The research of (Gandhi & Borse, 2004) showed that the inclusion of the <75 μm particles in the presence of larger size fractions led to a decrease in the material removal rate. This is thought to result from the fine particles forming a cushion layer on the surface and absorbing the impact of the larger and more energetic particles. So, to improve the accuracy of erosion models, it is necessary to include the distributions of particle sizes. The literature describes several functional forms (power, log, hyperbola, and exponential power) to mathematically model the distributions of particle sizes. An especially popular method is the Rosin-Rammler distribution (Rodríguez et al., 2016) as it includes a large range of materials, requires very few rate parameters, and in many cases, provides a better fit to the experimental data than competing models (K. Wang et al., 2017). Particles and carrier fluids can influence erosion in different ways. Erosion patterns can be quite different using different carrier fluids. In gas–solid flows, particles often leave the fluid streamlines, but in liquid–solid flows, particles stay on the streamlines (Mansouri et al., 2015). Erosion patterns depend on the inertial and drag forces on the particles. In liquid–solid erosion, the drag force will seam to guide particles to the side and reduce impacts with the wall, in turn reducing erosion. This is likely not true for gas–solid flows.

Different carriers can create different erosion patterns because of their unique ways of transporting particles. In gas-solid flows, erosion tends to create a characteristic "V" shape at elbow bends, as (Peng & Cao, 2016; Solnordal et al., 2015; Vieira et al., 2016) describe. On the other hand, liquid-solid flows create inconsistent erosion patterns because of fluid–particle interactivity, which greatly affects particle motion. These researchers all suggest the importance of understanding erosion patterns. Specifically, regarding the liquid-solid systems, they suggest understanding the nature of flow and the interaction of particles with the fluid, as well as accepting the geometric arrangement and complexity of the flow, as it can greatly affect the range of local flow behavior and patterns to nominate possible erosion. Under the right conditions, straight pipelines can be prone to erosion loss, but they're typically at a low risk because there are fewer particle interactions with the walls and material loss during flow is controlled.

Parts such as valves, tees, and elbows are more susceptible to erosion than straight sections of pipe; they encourage direct particle erosion and particle recirculation. Moreover, erosion behavior is highly sensitive to small geometric changes. (Chen et al., 2006) studied the erosion that occurs in elbows and plugged tees and concluded that in plugged tees, the severity of flow redirection is greater. In several instances, particles were observed to recirculate along almost the same trajectory in excess of 100 times and were repeatedly impacting the same location, resulting in extremely localized erosion. Each design and configuration has its own flow field, and the effect of flow and recirculation on material degradation can be both positive and negative. Due to this, the relationship between geometric design and erosion mitigation requires extensive studies.

The most recent erosion studies have centered on conventional elbow geometries since elbows are some of the most used fittings in process industries and petroleum production systems (Karimi et al., 2017; Parsi et al., 2017). However, research on different elbow orientations and bend angles is still lacking and is deserving of attention. Gas–solid–liquid three-phase flow is common in shale gas gathering and transportation, and in this case, the shale gas is the carrier phase. For example, in the Changning Shale Gas Field, a single well may produce sand at a rate of 10 t/day and water at a rate of 100–200 m^3/day. When the sand and water come into contact with the pipeline wall, an erosion–corrosion process synergistically occurs, which leads to the loss of pipe material and increases the cost to maintain the pipe. This situation also leads to significant loss of operation and safety (Q. Wang et al., 2022). Studies have shown that the 90° elbow is the section of the pipeline that is most vulnerable to erosion–corrosion damage in shale gas transportation systems.

In recent years, CFD has been used for several years, with recent Industrial applications CFD frameworks growing in Industrial applications, tools, and understanding as well. Analysis of discrete phase models for multiphase flow continues to be well documented, including how different parameters in the continuous phase numerically predict erosion, rate of erosion, and modifications of existing erosion models. Erosion scars (Chen et al., 2004), and erosion penetration rates in elbows have always been the mechanical properties of fluids (Oka et al., 2005), but are also the mechanical properties of fluids, plus the movement and trajectories of solid particles. Many earlier numerical studies of erosion prediction have been confined to simplistic conditions and did not consider fully how multiphase hydrodynamics influence the motion of particles. To complicate these factors, the CFD studies that have been done did not fully consider mechanical factors such as less inertial force, less drag force, Stokes number partitions, particle wall collisions of secondary particles in elbow erosion geometry, the distribution of sulfur particles and the movement of these particles.

The main goal of this project is to perform numerical simulations in order to build a knowledge base that can help learn about the mechanisms of erosion in multiphase flow systems using CFD. Moreover, the novelty of this work lies in the systematic evaluation of erosion characteristics in oil pipelines with different curvature angles using a two-way coupled CFD–DPM approach. In this research, four different configurations of oil pipelines are used to test the erosion rates using the multiphase flow models in ANSYS CFD. The development of erosion CFD models that can be modified to simulate the flow in pipelines, more specifically annular flows and multiphase slugs, is another goal, as they are highly relevant to the flow conditions of real pipelines.

Mathematical Representations

Problem Representation:

The pipe model geometry consisted of two (2) cylindrical straight pipe sections connected by a local geometry (elbow). The choice of pipe design was inspired by the geometric complexity associated with pipeline installation at offshore oil and gas production sites, in harmony with the terrain. Four (4) 3D pipe models were created in the SpaceClaim platform using the ANSYS 2020R1. The pipe designs are shown in Fig. 1. The dimensions used in designing the pipe geometries are the same, but the main difference between each design is the angle of curvature. The horizontal length of the pipe is 250 mm, and its radius is 50 mm. In the current study, four different angles were considered to represent oil pipe configurations. These angles are 45^o, 90^o, 135^o and 180^o. The four (4) pipe designs were named Case_1_(45^o), Case_2_(90^o), Case_3_(135^o) and Case_4_(180^o). Table 1 shows a summary of all parameters taken into account when creating the pipe geometry.

Table 1. Pipe model design parameters.

Parameter	Input
Pipe material	Steel
Normalized pipe radius	50 mm
Normalized straight length	250 mm
Curvature angle	45º, 90 º, 135 º and 180 º

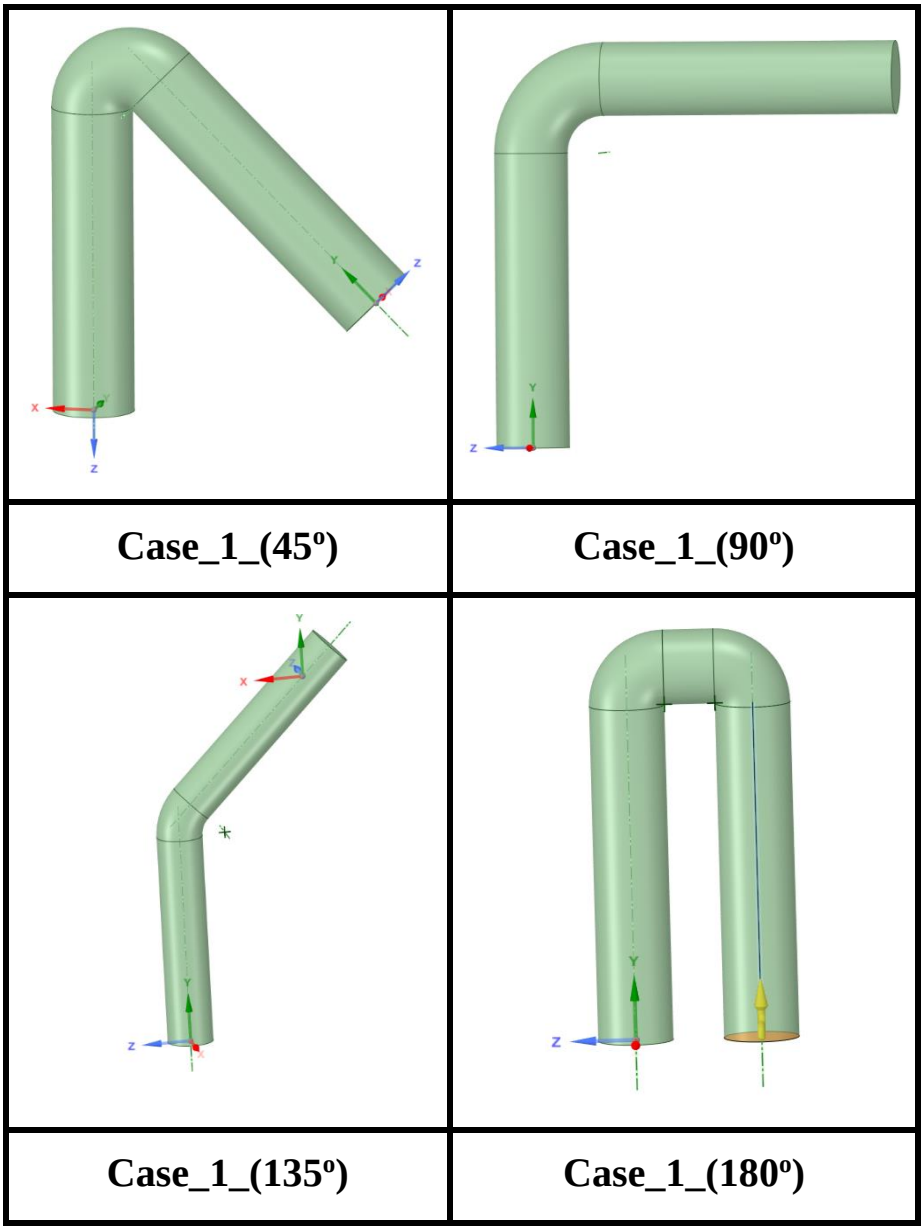

Fig. 1. Considered pipe model design for different curvature angles.

Boundary Conditions:

The last step of the flow modelling process requires the implementation of boundary conditions. Three boundary types were used in this study: velocity inlet, pressure outlet and wall. At the inlet, flow velocity was defined to be normal to the boundary, while the outlet was set to atmospheric pressure by applying zero-gauge pressure. The turbulence intensity of backflow and hydraulic diameter at the inlet and outlet were set to 5% and 0.072 m. The stationary no-slip wall boundary was used to define the elbow wall. The flow was also assumed to be turbulent and incompressible, as well as steady-state. A particle diameter of 100 μm was selected, which falls within the commonly reported size range encountered in oil and gas production systems and erosion studies. The particle density was specified as 2650 kg/m³, representing quartz sand, while the particle injection velocity was assumed to be equal to the local fluid velocity at the inlet.

Governing Equations:

Flow modelling is the first main step of CFD erosion prediction, which uses CFD codes to solve the governing Navier-Stokes equation or fluid motion equation. In this study, the Reynolds Stress Model (RSM) is used to solve the turbulence flow as below (Vanaki et al., 2016):

Continuity equation:

$$\nabla.\left(\rho_{nf}\vec{V}\right) = 0 \tag{1}$$

Momentum equation:

$$\nabla.\left(\rho_{nf}\vec{V}\vec{V}\right) = -\nabla p + \nabla\left(\mu_{nf}\nabla\vec{V}\right) + S_m \tag{2}$$

where S_m describes the momentum transfer between phases, which is calculated as:

$$S_m = \frac{1}{\delta V}\sum_{b=1}^{n}\vec{F}_b \tag{3}$$

In the *DPM*, the current numerical code foretells the path of the dispersed phase by integrating the balance of the acting force on the nanoparticles. Therefore, the equation of particle motion is expressed by the following formula as (Albojamal & Vafai, 2017):

$$m_P\frac{d\vec{V}_P}{dt} = F_D + F_g + F_L + F_{Br} + F_T + F_P + F_v \tag{4}$$

On the left-hand side of the above equation, m_p is the particle mass, $\vec{V}_P$ is the particle velocity vector, and the right-hand side symbolizes the forces acting on the particle, which are resistance, gravity, lift, Brownian, Thermophoresis, pressure gradient and virtual mass forces, respectively. More detailed information and correlations of these forces are provided in Ref (Vanaki et al., 2016).

Turbulence Modeling:

Many researchers have used the shear stress transfer (SST) model to simulate flow in roughened channels since this model presents compatible results with those of experimental data (Bianco et al., 2009). Therefore, the current simulation uses this model for curved pipes. The standard κ-ω turbulence model has the following equations (F. R. Menter, 1994):

$$\frac{\partial}{\partial x_i}\left(\rho_{nf}\kappa V_i\right) = \frac{\partial}{\partial x_j}\left\{\left(\mu_{nf} + \frac{\mu_t}{\sigma_\kappa}\right)\frac{\partial \kappa}{\partial x_j}\right\} + G_\kappa - \rho_{nf}\kappa\varpi\beta_1 \tag{5}$$

$$\frac{\partial}{\partial x_i}\left(\rho_{nf}\varpi V_i\right) = \frac{\partial}{\partial x_j}\left\{\left(\mu_{nf} + \frac{\mu_t}{\sigma_\varpi}\right)\frac{\partial \varpi}{\partial x_j}\right\} + G_\varpi - \rho_{nf}\varpi^2\beta_2 + (1 - F_1)\rho_{nf}\sigma_{\varpi,2}\frac{1}{\varpi}\frac{\partial \kappa}{\partial x_i}\frac{\partial \varpi}{\partial x_i} \tag{6}$$

where G_κ is the generation of the kinetic energy of turbulence due to the averaged velocity gradients, and G_ϖ represents the generation of ϖ.

The turbulent viscosity, μ_t is represented as:

$$\mu_t = \frac{\rho_{nf}\kappa}{\varpi}\frac{1}{max\left(\frac{1}{\alpha^*}, \frac{SF_2}{\alpha_1\varpi}\right)} \tag{7}$$

where F_1 and F_2 are the blending functions and S is the value of strain rate. In Eqs. (3.5) and (3.6), σ_κ and σ_ϖ are similar to the turbulent Prandtl numbers, *Pr*, which are determined as follows:

$$\sigma_\kappa = \frac{1}{\frac{F_1}{\sigma_{\kappa,1}} + \frac{(1-F_1)}{\sigma_{\kappa,2}}} \tag{8}$$

$$\sigma_\omega = \frac{1}{\frac{F_1}{\sigma_{\varpi,1}} + \frac{(1-F_1)}{\sigma_{\varpi,2}}} \tag{9}$$

The blending functions are defined by:

$$F_1 = \tanh(\emptyset_1^4) \tag{10}$$

$$F_2 = \tanh(\emptyset_2^2) \tag{11}$$

where,

$$\emptyset_1 = \min\left[\max\left(\frac{\sqrt{\kappa}}{0.09\varpi y}, \frac{500\mu}{\rho y^2 \varpi}\right), \frac{4\rho\kappa}{\sigma_{\varpi,2}D_\varpi^+ y^2}\right] \tag{12}$$

$$D_{\varpi}^{+} = \max\left[2\rho\frac{1}{\sigma_{\varpi,2}\varpi}\frac{\partial\kappa}{\partial x_j}\frac{\partial\varpi}{\partial x_j}10^{-20}\right] \quad (13)$$

$$\emptyset_2 = \max\left[\left(\frac{2\sqrt{\kappa}}{0.09\varpi y}, \frac{500\mu}{\rho y^2\varpi}\right)\right] \quad (14)$$

where y is the near-surface spacing and D_{ϖ}^{+} is the positive portion of the cross-diffusion term. The constants of this model are $\sigma_{\kappa,1} = 1.176$, $\sigma_{\varpi,1} = 2$, $\beta_1 = 0.075$, $\beta_2 = 0.0828$, $\alpha_1 = 0.31$, $\sigma_{\kappa,2} = 1$ and $\sigma_{\varpi,2} = 1.168$.

Erosion Modelling:

The third component will be the prediction of the erosion rate caused by sand particle impingements. The impact properties of each particle are stored in the cell next to the wall.

$$R_{\text{erosion}} = \sum_{p=1}^{N_{\text{particles}}} \frac{\dot{m}_p C(d_p) f(\alpha) v^{b(v)}}{A_{\text{face}}} \quad (15)$$

where $C(d_p)$ is the diameter function, $f(\alpha)$ is the impact angle function with α as the impact angle of the particle path with the wall face and $b(v)$ is the function of relative particle velocity. A_{face} is the area of the cell face at the wall (Nakasone et al., 2007). $f(\alpha)$ was determined based on the impact angle function for typical 'ductile' and 'brittle' material.

Grid Generation

The computational mesh was created using ANSYS Fluent's Directed Mesh Inflation technique, believed to be adequate for simulating two-phase flow within a horizontal pipe. This technique was adopted as it has the potential to minimize the computational effort and total number of mesh elements when compared with alternative techniques, in addition to being able to create structured multi-block grids in a parametric way. With the path mesh option, the number of divisions in the pipe inlet section is controlled, resulting in the generation of high-quality quadrilateral elements. The method of volume distribution used allows the total number of mesh layers along the pipe wall to be specified. The mesh configuration used in this study is shown in Fig. 2.

Solution Procedure

The finite volume method (FVM) was used to solve the governing equations and boundary conditions for the two-phase flow. ANSYS Fluent 2020 R1 was used for all numerical simulations. The PRESTO scheme was used for pressure calculations, and the QUICK scheme was used for volume fraction calculations. All other transport equations were discretized with the second-order upwind scheme. The SIMPLE algorithm was used for pressure–velocity coupling, and the Discrete Phase Model (DPM) was used with two-way coupling for the continuous and dispersed phases. The fluid was allowed to influence the particle motion by drag forces, and the particles also transferred momentum and energy to the surrounding fluid. Suitable under-relaxation factors were used on all dependent variables during the iterative process to maintain numerical stability and ensure convergence. The residuals of all governing equations were set to 10^{-5} to establish the convergence criterion.

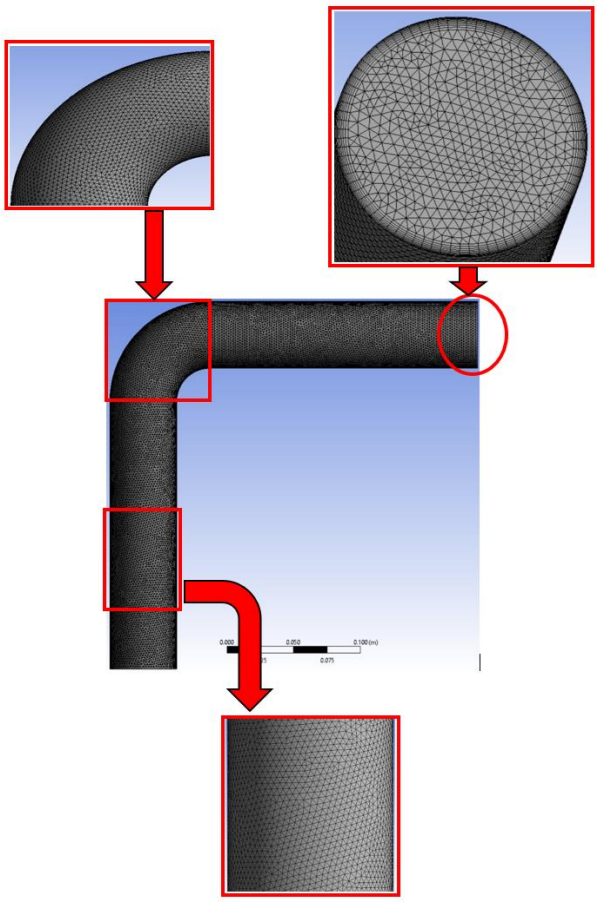

Fig. 2. Mesh generation of the present study.

Results and Discussion

The simulations are implemented to compute the influence of pipe configurations and flow velocity on fluid flow and erosion rate. In this regard, the CFD calculations are performed for a specific range of these parameters as follows: (20 m/s, 25 m/s, 30 m/s and 35 m/s) and pipe curvature angles of 45o, 90 o, 135 o and 180 o. The DPM model was considered for particle flow. These results are represented by pressure, velocity and corrosion rate contours. In addition, the average corrosion rate for all pipe configurations considered is presented for four different velocity values.

Fig. 3 shows the velocity contours for four different pipe configurations with the curvature angle of (45o, 90 o, 135 o and 180 o) at (A) Velocity (V)= 20 m/s and (B) Velocity (V)= 35 m/s. For V=45 m/s, the flow pattern within the pipe changes significantly. For example, this pipe induces stronger secondary flows and vortices, leading to more complex velocity distributions. For pipes with angles of 90° and 135°, we find that the flow from the fluid inlet to the outlet was almost uniform, with large values observed at the deviation angle. For the pipe with a deviation angle of 180o, we find that the flow was uniform at the entrance but irregular at the exit. We notice that the velocity distribution on the right side of the exit is always higher than on the left side. Changing the velocity flow in an elbow pipe has significant implications for flow characteristics and the overall performance and durability of the piping system. Therefore, engineers must carefully consider these effects when designing and operating fluid handling systems to optimize efficiency, minimize energy consumption, and ensure the integrity of the equipment.

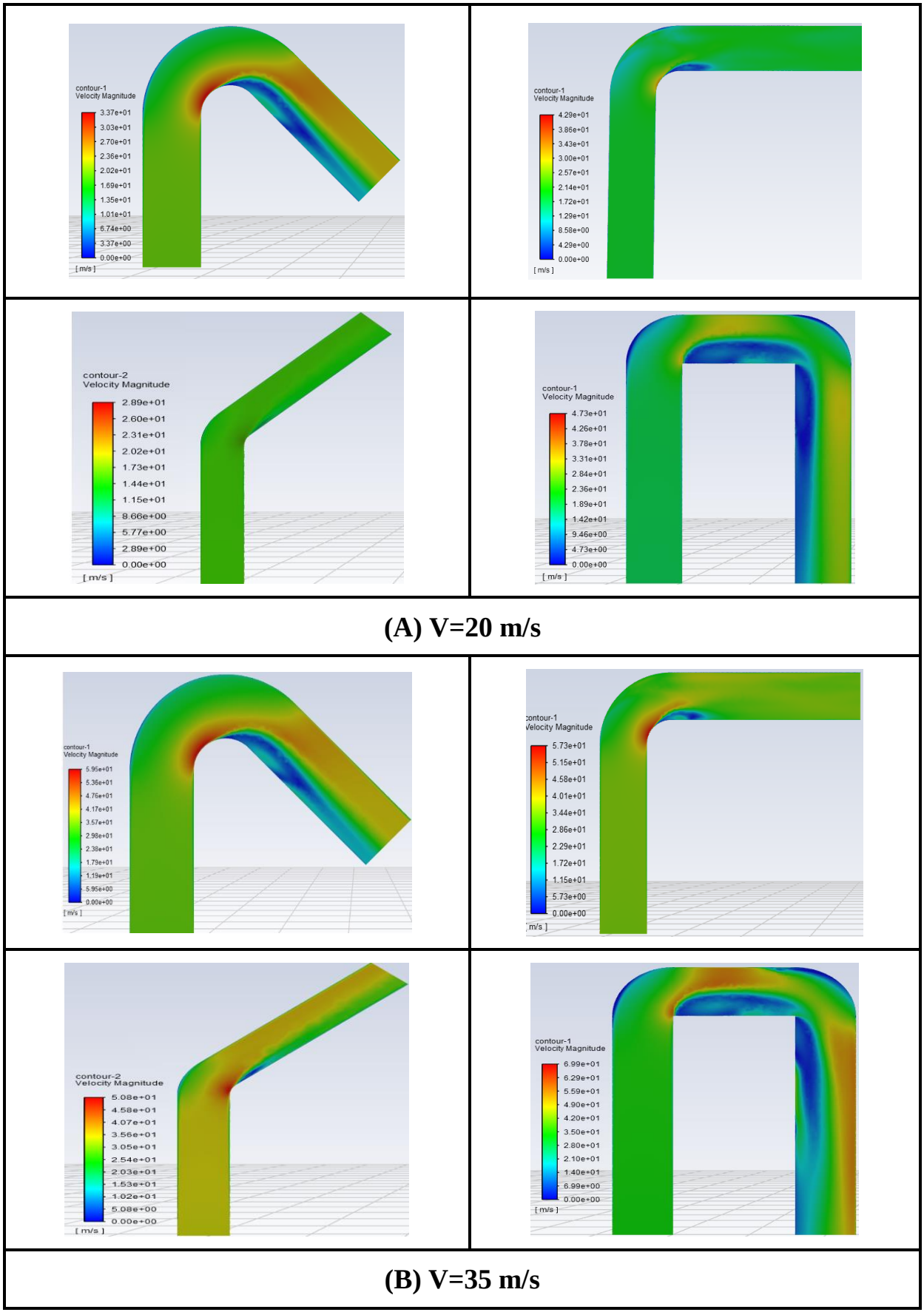

Fig. 3. Velocity contours for all studied pipe configurations at (A) V=20 m/s and (B) V=35 m/s.

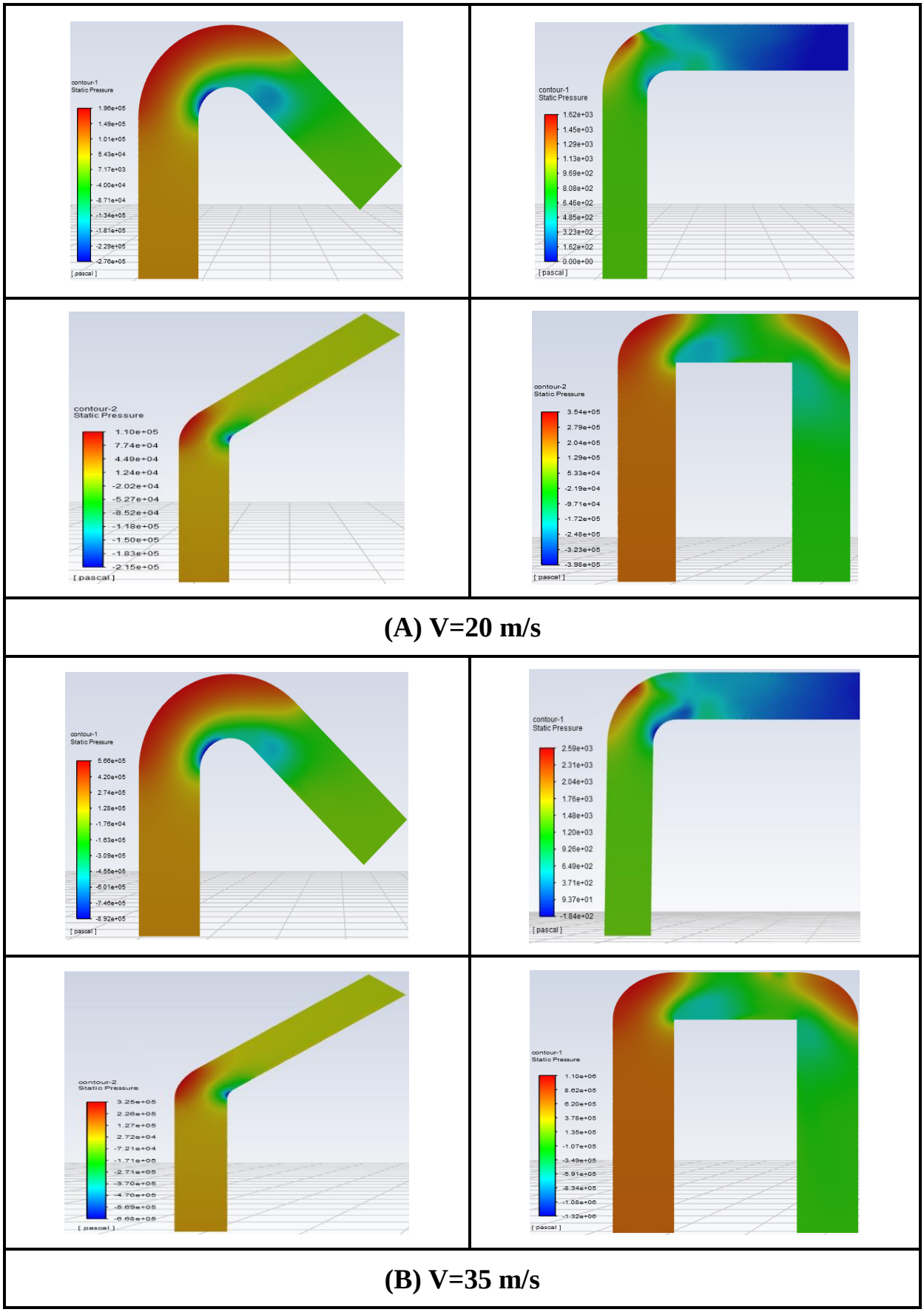

Fig. 4. Pressure contours for all studied pipe configurations at (A) V=20 m/s and (B) V=35 m/s.

Fig. 4 shows the pressure contours for four different pipe configurations with the curvature angle of (45^{o}, 90 ^{o}, 135 ^{o} and 180 ^{o}) at (A) Velocity (V)= 20 m/s and (B) Velocity (V)= 35 m/s. Through meticulous examination of the illustration, it is plausible to infer that the fluid pressure tends to be elevated in regions characterized by minimal flow velocity estimations. This pattern was consistent across all four (4) pipe configurations and was particularly pronounced in the case of Case_1_(180^{o}). Changing the velocity flow in an elbow pipe alters the pressure distribution within the system, affecting factors such as pressure gradients, pressure drop, secondary flow patterns, and energy consumption. Understanding these effects is crucial for designing efficient piping systems and optimizing the performance of fluid handling processes.

Fig. 5 shows the erosion rate contours for four different pipe configurations with the curvature angle of (45 °, 90 ^{o}, 135 ^{o} and 180 ^{o}) at (A) Velocity (V)= 20 m/s and (B) Velocity (V)= 35 m/s. From these contours, we see that the corrosion rate is concentrated in the curves for all pipe configurations and increases significantly as velocity increases. Changes in flow velocity within an elbow pipe can have a significant impact on erosion distribution. Higher velocities can lead to increased erosion severity, wider erosion distribution, and the formation of erosion hotspots within the elbow. Understanding these effects is crucial for mitigating erosion damage and designing erosion-resistant piping systems, particularly in applications involving abrasive fluids.

The results in Fig. 6 represent the erosion rates with various configurations of pipelines along with the increase in inlet velocity from 20 m/s to 35m/s. For all lines, there is an increase in trend with their linesal movement increasing from a velocity of 20 m/s to a velocity of 35 m/s. The pipeline of the 45 ° portion (red) is always to the right of the others. It is the most severe for recorded alterations in erosion at the velocity intervals of 20 m/s to 35 m/s. The 45-degree angle is an outlier in the acceleration of the line because of a a 14% increase in erosion velocity. It can be aligned to the fact that sharper bend angles, such as the 45-degree angle, give a more changeable flow of gas, which causes increased mitigation of wall erosion along with sharper collisions with flowable particles along the gas. The 90-degree portion (green) of the figure is at the opposite end of the severity for rising erosion, with an increase of only 2% along the recorded velocity intervals of 20 m/s to 35 m/s. The 90-degree bend is superior for line flow balance, along with the improvement of distribution of line flow, which reduces the overall line erosion occurring from the gas flow. The 135-degree portion (blue) is in the middle for recorded increases along the observed intervals along the velocity ring, with a recorded alteration 4% along the recorded velocity intervals. The 180-degree portion (grey) of the gas line improves the severity of gas line erosion, having the strongest recorded alteration of 11% for the observed velocity intervals. The figure gives evidence of increasing speeds, along with sharp line bends, which increase gas line erosion.

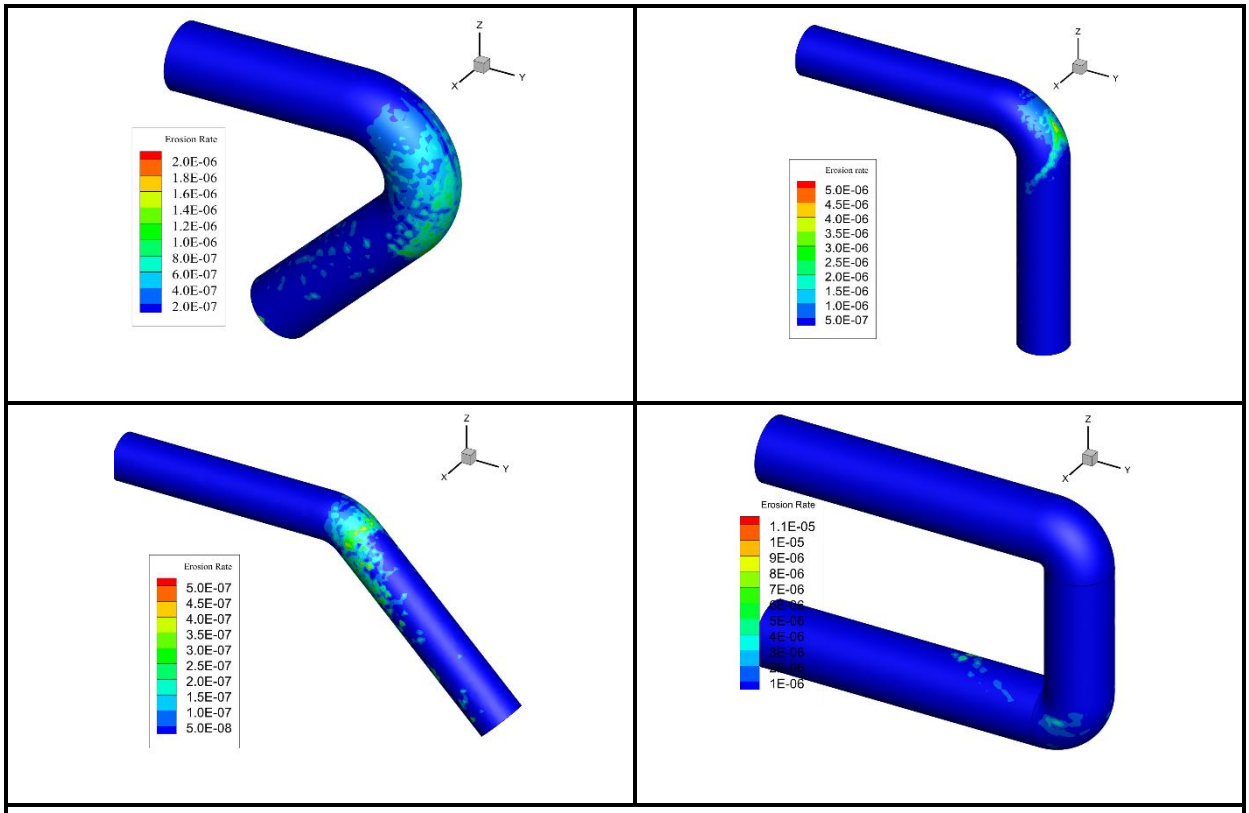

(A) V=20 m/s

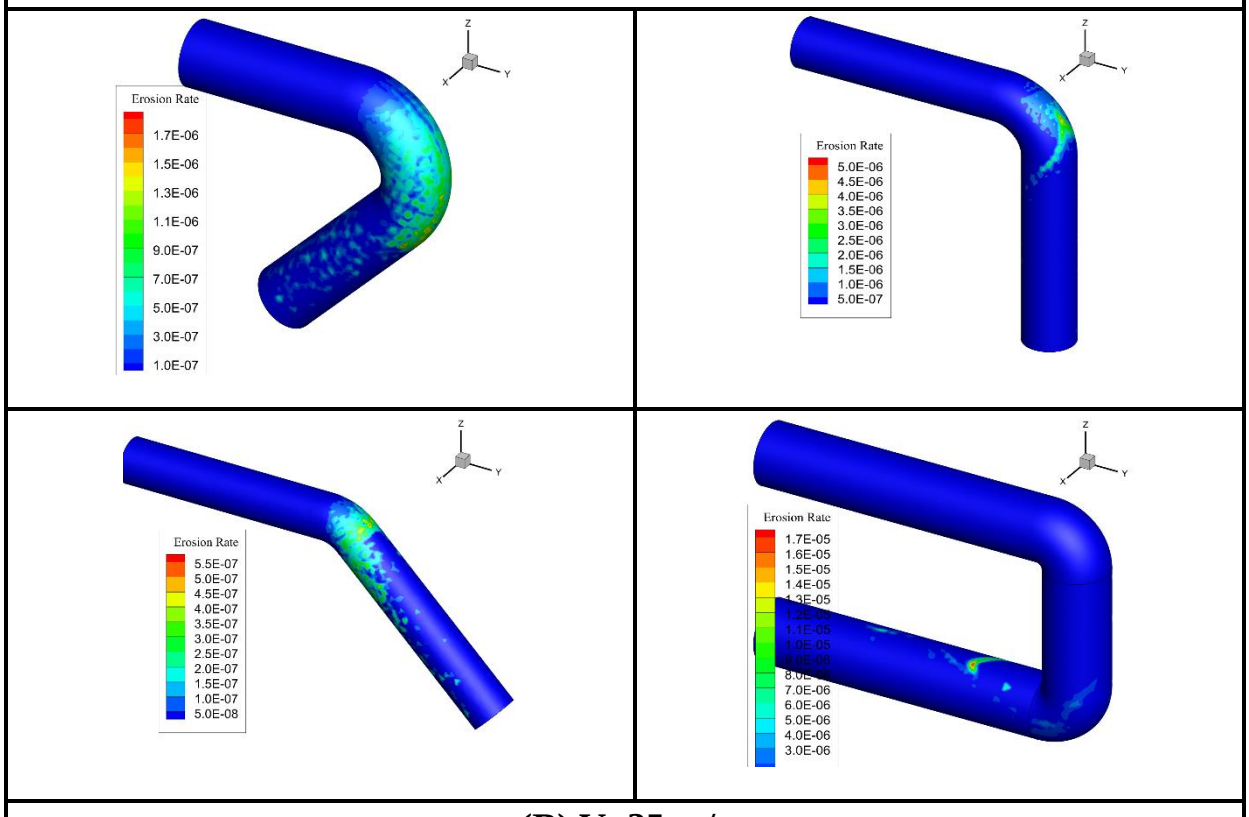

(B) V=35 m/s

Fig. 5. Erosion rate contours for all studied pipe configurations at (A) V=20 m/s and (B) V=35 m/s.

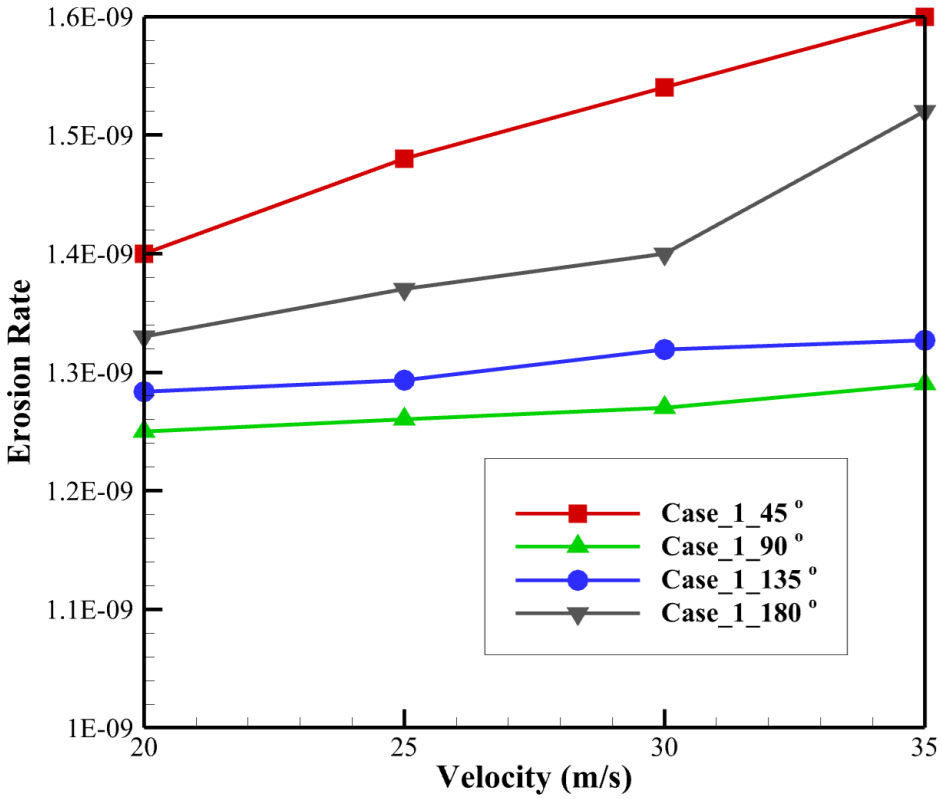

Fig. 6. Erosion rate values as a function of inlet velocity for all pipe configurations.

Conclusion

A computational fluid dynamics (CFD) model coupled with a discrete phase model (DPM) was successfully applied to investigate erosion behavior in four oil pipeline configurations under different flow velocities and bend angles. The simulation results demonstrated that the erosion rate increased with increasing inlet velocity, confirming the strong influence of flow conditions on pipeline wear. Among the investigated configurations, the 45° bend exhibited the highest average erosion rate, whereas the 90° bend showed the lowest erosion rate. At an inlet velocity of 35 m/s, the erosion rate for the 45° configuration was approximately 24% higher than that of the 90° configuration, highlighting the significant effect of bend angle on erosion characteristics. These findings provide valuable insights for optimizing pipeline design and reducing erosion-related failures in crude oil transportation systems.

References

Albojamal, A., & Vafai, K. (2017). Analysis of single phase, discrete and mixture models, in predicting nanofluid transport. *International Journal of Heat and Mass Transfer*, *114*, 225–237. https://doi.org/10.1016/j.ijheatmasstransfer.2017.06.030

Bianco, V., Chiacchio, F., Manca, O., & Nardini, S. (2009). Numerical investigation of nanofluids forced convection in circular tubes. *Applied Thermal Engineering*, *29*(17–18),

3632–3642. https://doi.org/10.1016/j.applthermaleng.2009.06.019

Chen, X., McLaury, B. S., & Shirazi, S. A. (2004). Application and experimental validation of a computational fluid dynamics (CFD)-based erosion prediction model in elbows and plugged tees. *Computers and Fluids*, *33*(10), 1251–1272. https://doi.org/10.1016/j.compfluid.2004.02.003

Chen, X., McLaury, B. S., & Shirazi, S. A. (2006). Numerical and experimental investigation of the relative erosion severity between plugged tees and elbows in dilute gas/solid two-phase flow. *Wear*, *261*(7–8), 715–729. https://doi.org/10.1016/j.wear.2006.01.022

Ejeh, C. J., Boah, E. A., Akhabue, G. P., Onyekperem, C. C., Anachuna, J. I., & Agyebi, I. (2020). Computational fluid dynamic analysis for investigating the influence of pipe curvature on erosion rate prediction during crude oil production. *Experimental and Computational Multiphase Flow*, *2*(4), 255–272. https://doi.org/10.1007/s42757-019-0055-5

F. R. Menter. (1994). Two-Equation Eddy-Viscosity Turbulence Models for Engineering Applications. *AIAA Journal*, *32*(8), 1598–1605.

Gandhi, B. K., & Borse, S. V. (2004). Nominal particle size of multi-sized particulate slurries for evaluation of erosion wear and effect of fine particles. *Wear*, *257*(1–2), 73–79. https://doi.org/10.1016/j.wear.2003.10.013

Hamzah, H., & Sahin, B. (2023). Analysis of SWCNT-water nanofluid flow in wavy channel under turbulent pulsating conditions: Investigation of homogeneous and discrete phase models. *International Journal of Thermal Sciences*, *184*. https://doi.org/10.1016/j.ijthermalsci.2022.108011

Hamzah, H., Zontul, H., & Sahin, B. (2025). Exploring Homogeneous and Discrete Models for Predicting Hydrothermal Flow and Entropy Generation. *Heat Transfer Engineering*. https://doi.org/10.1080/01457632.2025.2489706

Karimi, S., Shirazi, S. A., & McLaury, B. S. (2017). Predicting fine particle erosion utilizing computational fluid dynamics. *Wear*, *376–377*, 1130–1137. https://doi.org/10.1016/j.wear.2016.11.022

Kesana, N. R. (2013). *Erosion in multiphase pseudo slug flow with emphasis on sand sampling and pseudo slug characteristics*. 463.

Ludema, K. (1995). Wear models and predictive equations: Their form and content. *Wear*, *181–183*, 443–457. https://doi.org/10.1016/0043-1648(94)07102-0

Mansouri, A., Arabnejad, H., Karimi, S., Shirazi, S. A., & McLaury, B. S. (2015). Improved CFD modeling and validation of erosion damage due to fine sand particles. *Wear*, *338–339*, 339–350. https://doi.org/10.1016/j.wear.2015.07.011

Mcl Clark, H. (1991). On the impact rate and impact energy of particles in a slurry pot erosion tester. *Wear*, *146*, 165–183.

Nakasone, Y., Yoshimoto, S., & Stolarski, T. A. (2007). Engineering Analysis with ANSYS Software. *Engineering Analysis with ANSYS Software*, 1–456. https://doi.org/10.1016/B978-0-7506-6875-0.X5030-3

Neville, A., Reza, F., Chiovelli, S., & Revega, T. (2005). Erosion-corrosion behaviour of WC-based MMCs in liquid-solid slurries. *Wear*, *259*(1–6), 181–195. https://doi.org/10.1016/j.wear.2005.02.037

Oka, Y. I., Okamura, K., & Yoshida, T. (2005). Practical estimation of erosion damage caused by solid particle impact: Part 1: Effects of impact parameters on a predictive equation. *Wear*, *259*(1–6), 95–101. https://doi.org/10.1016/j.wear.2005.01.039

Parsi, M., Al-Sarkhi, A., Kara, M., Sharma, P., McLaury, B. S., & Shirazi, S. A. (2017). A new dimensionless number for solid particle erosion in natural gas elbows. *Wear*, *390–391*, 80–83. https://doi.org/10.1016/j.wear.2017.07.005

Peng, W., & Cao, X. (2016). Numerical prediction of erosion distributions and solid particle trajectories in elbows for gas-solid flow. *Journal of Natural Gas Science and Engineering*, *30*, 455–470. https://doi.org/10.1016/j.jngse.2016.02.008

Rodríguez, B. Á., García, G. G., Coello-Velázquez, A. L., & Menéndez-Aguado, J. M. (2016). Product size distribution function influence on interpolation calculations in the Bond ball mill grindability test. *International Journal of Mineral Processing*, *157*, 16–20. https://doi.org/10.1016/j.minpro.2016.09.004

Shirazi, S. A., Mclaury, B. S., Shadley, J. R., Roberts, K. P., Rybicki, E. F., Rincon, H. E., Hassani, S., Al-Mutahar, F. M., & Al-Aithan, G. H. (2015). Erosion-Corrosion in Oil and Gas Pipelines. *Oil and Gas Pipelines: Integrity and Safety Handbook*, 399–422. https://doi.org/10.1002/9781119019213.ch28

Solnordal, C. B., Wong, C. Y., & Boulanger, J. (2015). An experimental and numerical analysis of erosion caused by sand pneumatically conveyed through a standard pipe elbow. *Wear*, *336–337*, 43–57. https://doi.org/10.1016/j.wear.2015.04.017

Subramani, H. J., Rhyne, L. D., & Vedapuri, D. (2014). Sand fines erosion and asset integrity management. *Proceedings of the Annual Offshore Technology Conference*, *3*, 2306–2311. https://doi.org/10.2118/24944-ms

Vanaki, S. M., Ganesan, P., & Mohammed, H. A. (2016). Numerical study of convective heat transfer of nanofluids: A review. *Renewable and Sustainable Energy Reviews*, *54*, 1212–1239. https://doi.org/10.1016/j.rser.2015.10.042

Vieira, R. E., Mansouri, A., McLaury, B. S., & Shirazi, S. A. (2016). Experimental and computational study of erosion in elbows due to sand particles in air flow. *Powder Technology*, *288*, 339–353. https://doi.org/10.1016/j.powtec.2015.11.028

Wang, K., Li, X., Wang, Y., & He, R. (2017). Numerical investigation of the erosion behavior in elbows of petroleum pipelines. *Powder Technology*, *314*, 490–499. https://doi.org/10.1016/j.powtec.2016.12.083

Wang, Q., Ba, X., Huang, Q., Wang, N., Wen, Y., Zhang, Z., Sun, X., Yang, L., & Zhang, J. (2022). Modeling erosion process in elbows of petroleum pipelines using large eddy simulation. *Journal of Petroleum Science and Engineering*, *211*. https://doi.org/10.1016/j.petrol.2022.110216

Wee, S. K., & Yap, Y. J. (2019). CFD study of sand erosion in pipeline. *Journal of Petroleum Science and Engineering*, *176*, 269–278. https://doi.org/10.1016/j.petrol.2019.01.001